arXiv:1704.07884v1 [cond-mat.mtrl-sci] 25 Apr 2017

Decomposition mechanisms in metal borohydrides and their ammoniates

Evan Welchman[a] and Timo Thonhauser[a,b,c]

Ammoniation in metal borohydrides (MBs) with the form $\mathscr{M}(BH_4)_x$ has been shown to lower their decomposition temperatures with $\mathscr{M}$ of low electronegativity ($\chi_p \lesssim 1.6$), but raise it for high-χ_p MBs ($\chi_p \gtrsim 1.6$). Although this behavior is just as desired, an understanding of the mechanisms that cause it is still lacking. Using *ab initio* methods, we elucidate those mechanisms and find that ammoniation always causes thermodynamic destabilization, explaining the observed lower decomposition temperatures for low-χ_p MBs. For high-χ_p MBs, we find that ammoniation blocks B_2H_6 formation—the preferred decomposition mechanism in these MBs—and thus kinetically stabilizes those phases. The shift in decomposition pathway that causes the distinct change from destabilization to stabilization around $\chi_p = 1.6$ thus coincides with the onset of B_2H_6 formation in MBs. Furthermore, with our analysis we are also able to explain why these materials release either H_2 or NH_3 gas upon decomposition. We find that NH_3 is much more strongly coordinated with higher-χ_p metals and direct H_2 formation/release becomes more favorable in these materials. Our findings are of importance for unraveling the hydrogen release mechanisms in an important new and promising class of hydrogen storage materials, allowing for a guided tuning of their chemistry to further improve their properties.

1 Introduction

Hydrogen is an ideal energy carrier in a clean energy system,[1–3] but there is no known material to economically and safely store hydrogen in a package sufficiently small and hydrogen-dense for use in mobile applications. In the search for a material that meets the US Department of Energy's targets for a practical hydrogen storage material,[4,5] metal borohydrides (MBs) have seen a surge of interest[6–11] and remain one of the most promising classes of hydrogen storage materials.[12] In recent years, various studies have found that these metal borohydrides typically demonstrate improved hydrogen storage properties when complexed with ammonia, forming a new class of materials called metal borohydride ammoniates (MBAs).[13–18] Generally, MBAs tend to release hydrogen gas at more practical temperatures and greater purity than their plain MB counterparts.[13] Furthermore, recent experiments have mixed various MBAs with MBs or ammonia borane (NH_3BH_3) to tune the H_2 release temperature and purity.[19,20]

Looking at the available experimental data for a large number of MBAs, a clear pattern emerges between the Pauling electronegativity χ_p of the metal $\mathscr{M}$ in $\mathscr{M}(BH_4)_x$ and the material's decomposition temperature.[21] As can be seen in Fig. 1, ammoniating a MB lowers the decomposition temperature of an MBA based on a metal with electronegativity $\chi_p \lesssim 1.6$, but stabilizes an MBA based on a high-electronegativity metal with $\chi_p \gtrsim 1.6$. While this experimental observation constitutes significant progress towards improved hydrogen storage materials, the underlying mechanism causing it is not understood. As such, further systematic improvements beyond simple trial-and-error attempts are challenging. In this paper, we present possible solutions and describe mechanisms that cause the ammoniation to "magically" destabilize just those MBs that need it, while stabilizing those that benefit from a higher decomposition temperature.

Focusing on decomposition temperature alone, however, oversimplifies the understanding of how these materials decompose. There are competing decomposition mechanisms for each of these materials, resulting in different gaseous products—mostly either NH_3 or H_2. These products have been included in Fig. 1 and split the destabilized set of materials into two distinct groups: those with low electronegativity ($\chi_p \lesssim 1.2$) that release mostly NH_3 in open systems and those with medium electronegativity ($1.2 \lesssim \chi_p \lesssim 1.6$) that may release NH_3 at lower temperatures and then transition to releasing mostly H_2 at higher temperatures.

In the decomposition pathway releasing ammonia, the thermodynamics are such that releasing ammonia gas is more favorable than remaining in the MBA structure.[22] As we will discuss in detail below, our data indicates that the ammonia is more weakly bound to the metal in MBAs where $\mathscr{M}$ has lower electronegativity. At the temperature where this process occurs, the remaining MBA (or plain MB) is below its decomposition temperature, and

[a]*Department of Physics, Wake Forest University, Winston-Salem, NC 27109, USA.*
[b]*Department of Chemistry, Massachusetts Institute of Technology, Cambridge, MA 02139, USA*
[c]*thonhauser@wfu.edu*

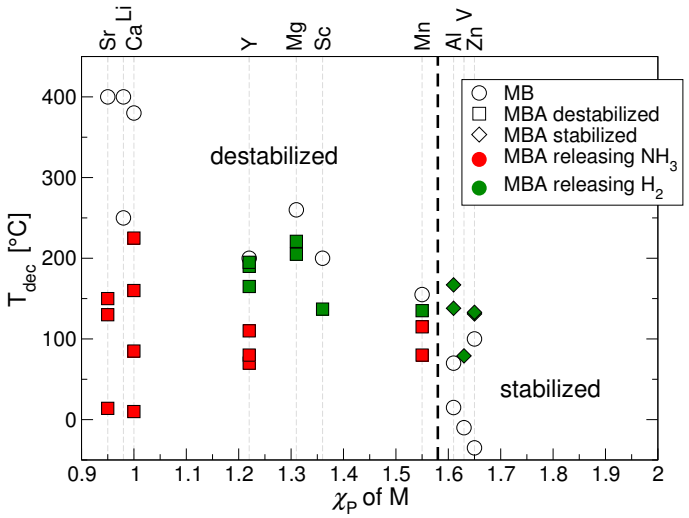

Fig. 1 Experimentally observed decomposition temperatures T_{dec} for selected MBs and MBAs plotted as a function of the electronegativity χ_p of the metal. Red-filled symbols indicate that a material releases mostly NH_3, while green-filled symbols indicate the release of mostly H_2. Materials to the left of the dashed line (squares) are thermally destabilized by ammoniation, to the right (diamonds) they are stabilized. Data adapted from Jepsen et. al.[13,22]

the MBA will not break down further. In high-electronegativity MBs ($\chi_p \gtrsim 1.6$), ammoniation raises the material's decomposition temperature relative to the plain MB and it was suggested that this behavior is linked to the creation of a heteropolar dihydrogen bond network between the negatively charged $H^{\delta-}$ in $[BH_4]^-$ and positively charged $H^{\delta+}$ in NH_3.[23] It is also known that the MBs in this category often decompose to release diborane (B_2H_6),[24] but this diborane is not released as a gaseous product in the presence of NH_3.[25] Instead, it likely acts as an intermediate, reacting with NH_3 to form boron nitrides as well as H_2.[9–11]

The decomposition of most MBs is a complicated process that is difficult to model with *ab initio* methods, as the correct intermediate structures are often unknown. Jena et al. have tried to identify likely intermediate structures in the borohydride decomposition by simulating the structures of B_nH_m clusters.[26] In the specific context of Mg borohydrides, Wolverton and co-workers have used a Monte Carlo-based structure-search method to find the most likely intermediate structures.[27] Another approach to explaining decomposition mechanisms in complex metal hydrides has been to simulate native defect formation in e.g. $LiNH_2$[28] and $LiBH_4$.[29] While these approaches have provided valuable insight and understanding of the decomposition processes in complex metal hydrides, the results may not directly apply to MBAs. A greater understanding of precisely how and why these materials decompose will yield insight into how to design an ideal hydrogen storage medium from this already attractive class of materials.

This work aims to elucidate various aspects of the underlying mechanisms responsible for the decomposition processes in MBAs. To this end, this manuscript is structured in the follwing way: First, we examine the dihydrogen bond network of these materials and find that it varies slightly with electronegativity, but cannot explain the sharp distinction between destabilization and stabilization observed in Fig. 1. Next, we analyze the thermodynamical stability and find that ammoniation always leads to a lowering of stability. While that explains the lowering of materials with $\chi_p \lesssim 1.6$ in Fig. 1, it does not explain the stabilization for $\chi_p \gtrsim 1.6$. Finally, directly simulating the hydrogen release process, we find that those high-χ_p materials get kinetically stabilized in that ammoniation blocks the usual decomposition pathway. The exact mechanism is material dependent and we will explain it on a case-by-case basis.

2 Computational Details

We performed calculations using density-functional theory (DFT) as implemented in VASP,[30–32] using the included projector augmented wave (PAW) pseudopotentials and a plane wave energy cutoff of 500 eV. We converged self-consistent energies to at least 10^{-5} eV and relaxed all atomic positions until all forces dropped below 10 meV/Å. Because of different unit cell sizes, k-point meshes varied, but all used Γ centered Monkhorst-Pack meshes automatically generated in VASP with at least $20b$ k-points in each direction, where b is the length of the reciprocal lattice vector in $Å^{-1}$. We used the vdW-DF1 density-functional[33–36] to properly account for the van der Waals interactions in the dihydrogen bond networks in these materials.

We performed transition-state searches in VASP using the climbing image nudged elastic band (NEB) method implemented in the VTST package.[37,38] In the case of B_2H_6 formation, we generated end-point structures for these calculations by bringing together nearby BH_4 molecules in the ground-state structures in a directed perturbation of the system to form a stable B_2H_6 molecule in the structure. This was done through an automated process that first moved the BH_4 molecules away from the metal cation or cations to which they were coordinated and then formed a B_2H_6 molecule along the axis between the moved BH_4 molecules. The remaining two H atoms were moved to the original locations of the BH_4 molecules. These structures were then allowed to relax until all ionic forces dropped below 10 meV/Å.

In most cases, crystal structures are taken from experiment, but in some cases we drew from theoretical work. Corresponding references are given in Table 1. For transition-state searches, we expanded any structures containing only one formula unit into a 2×2×2 supercell in order to avoid too much distortion in the crystal structure.

3 Results and Discussion

3.1 Examining the dihydrogen bond network

A first attempt to explain the peculiar effect that ammoniation has on the decomposition in Fig. 1 is to study the dihydrogen bond networks in these materials. All MBA materials contain networks of heteropolar dihydrogen bonds ($H^{\delta-}\cdots H^{\delta+}$) and it has been suggested that the proximity of the protic N–H and hydridic B–H allows H_2 creation through the simple combination of $H^{\delta+}$ and $H^{\delta-}$.[13,23] In low-χ_p materials, this combination process is suspected to be a possible hydrogen production mechanism,[43] and it was proposed that stabilization of high-χ_p materials may be due to shielding of the metal.[16,43] The dihydrogen bonds clearly play

Table 1 Sources for the starting structures of MBs and MBAs studied in this work.

MB / MBA	Ref.	MB/ MBA	Ref.
$Sr(BH_4)_2{\cdot}4NH_3$	25	$Mg(BH_4)_2{\cdot}2NH_3$	23
$Sr(BH_4)_2{\cdot}2NH_3$	25	$Mg(BH_4)_2$	39
$Sr(BH_4)_2{\cdot}NH_3$	25	$Zr(BH_4)_4{\cdot}8NH_3$	40
$Sr(BH_4)_2$	41	$Zr(BH_4)_4$	42
$Ca(BH_4)_2{\cdot}4NH_3$	25	$Mn(BH_4)_2{\cdot}3NH_3$	43
$Ca(BH_4)_2{\cdot}2NH_3$	25	$Mn(BH_4)_2{\cdot}2NH_3$	43
$Ca(BH_4)_2{\cdot}NH_3$	25	$Mn(BH_4)_2$	24
$Ca(BH_4)_2$	44	$Al(BH_4)_3{\cdot}6NH_3$	45
$Y(BH_4)_3{\cdot}7NH_3$	22	$Al(BH_4)_3$	24
$Y(BH_4)_3{\cdot}6NH_3$	22	$Zn(BH_4)_2{\cdot}2NH_3$	15
$Y(BH_4)_3{\cdot}5NH_3$	22	$Zn(BH_4)_2$	24
$Y(BH_4)_3{\cdot}4NH_3$	22	$NaZn(BH_4)_3{\cdot}2NH_3$	46
$Y(BH_4)_3{\cdot}2NH_3$	22	$Li_2Mg(BH_4)_4{\cdot}6NH_3$	47
$Y(BH_4)_3{\cdot}NH_3$	22	$Li_2Al(BH_4)_5{\cdot}6NH_3$	48
$Y(BH_4)_3$	49		

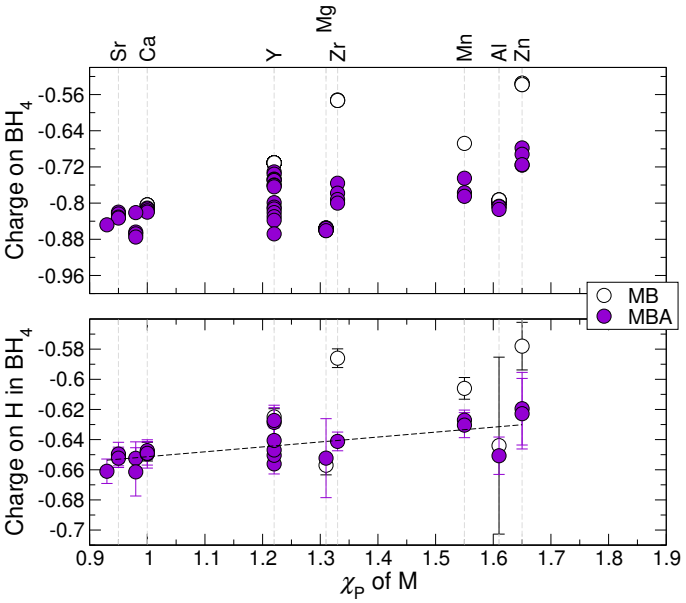

Fig. 2 (top) Bader charge [in units of e] on $[BH_4]^-$ anions relative to a neutral BH_4 molecule vs. χ_p of the metal cation with which they are coordinated. A perfect $[BH_4]^-$ anion would show a charge of -1. (bottom) Bader charge on $H^{\delta-}$ in $[BH_4]^-$ anions relative to a neutral H atom. Error bars indicate one standard deviation from the mean. Dashed lines indicate linear fits for the mean values for MBAs.

some role in determining the stability of these materials, as well as their decomposition, and further investigation is warranted.

We start by analyzing these interactions through a charge partitioning scheme and study how charge is distributed between the H atoms and the small molecules in which they reside. Figures 2 and 3 show the Bader charge[50,51] of BH_4 and NH_3 molecules in all MBAs from Table 1 relative to neutral molecules of the same composition. The plots show that the metal's electronegativity weakly affects the charge distribution in these molecules. Higher electronegativity results in weaker $[BH_4]^-$ anions and NH_3 molecules that begin to share charge with other constituents of the material.

On the level of individual H atoms, Fig. 2 shows that some materials demonstrate relatively large variations in the charge held by H atoms in the same molecule. This variation is likely due to how the molecules stack to form a crystal structure; the structure of $Al(BH_4)_3$ is built from $Al(BH_4)_3$ units where each BH_4 coordinates to only one Al atom, but the BH_4 units in $Zn(BH_4)_2$ act as bridges between multiple Zn atoms. Consequently, the charge on a BH_4 anion in $Al(BH_4)_3$ is more concentrated on one side of the molecule, giving the H atoms in $Al(BH_4)_3$ a larger variation in charge than those in $Zn(BH_4)_2$.

We also investigated the effect of H···H bond length on how much charge builds up on the H atoms in these materials; one might expect that shorter bond lengths would draw stronger relative charges for $H^{\delta+}$ and $H^{\delta-}$. Figure 4 shows that $H^{\delta+}$ in NH_3 on average does draw more charge when involved in shorter dihydrogen bonds, but the relationship is weak and $H^{\delta-}$ shows no relationship at all. To demonstrate the strength of this relationship, we modeled the dihydrogen bond as a Coulomb interaction ($q_1 q_2/r^2$ with calculated Bader charges of $H^{\delta+}$ and $H^{\delta-}$ as q_1 and q_2). Figure 5 shows that the data points fall almost perfectly along a fit generated by using the average $H^{\delta+}$ and $H^{\delta-}$ charges that we calculated from all MBAs included in Table 1. Thus, bond length has a weak effect on charge buildup on $H^{\delta+}$ atoms, and the corresponding increase in the electrostatic force across the bond is very small. This means that there is almost no additional charge polarization across the NH_3 and $[BH_4]^-$ molecules due to short dihydrogen bond lengths and any significant effects are localized to the electron clouds around the H atoms.

To summarize, χ_p and the specific geometry of the structure are more important for determining the charge distribution in the material than bond lengths. These results indicate that the dihydrogen bond network is very similar between different MBAs. While the dihydrogen bond network may play an important role in the decomposition process, that role does not appear to be linked in an obvious way with χ_p. It follows that variations (by themselves) in the dihydrogen bond network from one MBA to another cannot explain the distinct destabilizing/stabilizing effect of ammoniation observable in Fig. 1.

3.2 Examining thermodynamic stability

Moving beyond the dihydrogen bond network, we next examine the thermodynamics of the ammoniation process by calculating the energy of formation for both MB and MBA materials relative to their constituents in their natural states (i.e. the appropriate, separate amounts of solid $\mathscr{M}$ and B, and gaseous N_2 and H_2). The results are given in Table 2 and shown graphically in Fig. 6.

The primary result from these data is that all MBAs are thermodynamically destabilized relative to their plain MB counterparts. Furthermore, sequential events of NH_3 release from the same structure typically results in a MBA with lower energy of formation per atom. For instance, $Sr(BH_4)_2{\cdot}4NH_3$ may decompose by releasing $2NH_3$, leaving $Sr(BH_4)_2{\cdot}2NH_3$, which has a lower energy of formation per atom.

Note that NH_3 release in these materials is frequently accompanied by an endothermic event,[25,43] whereas lowering energy per

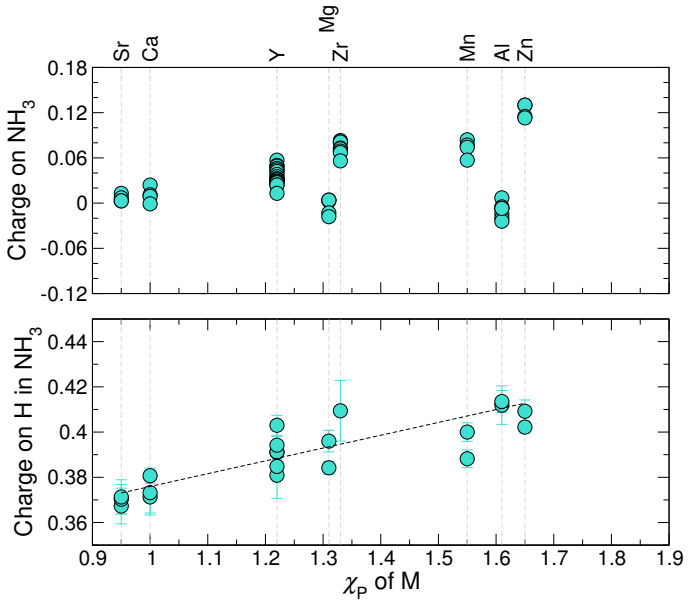

Fig. 3 (top) Bader charge [in units of e] on NH_3 molecules relative to a neutral NH_3 molecule vs. χ_p of the metal cation with which they are coordinated. (bottom) Bader charge relative to a neutral H atom for $H^{\delta+}$ in NH_3 molecules. Error bars indicate one standard deviation from the mean. Dashed lines indicate linear fits for the mean values for MBAs.

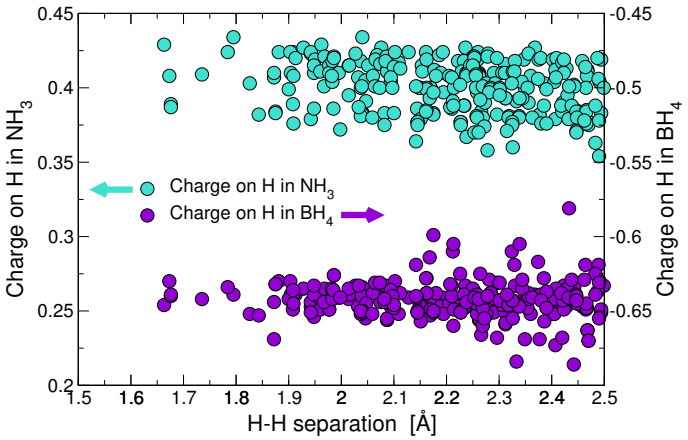

Fig. 4 Bader charge [in unites of e] on H atoms in NH_3 and BH_4 molecules that are part of heteropolar dihydrogen bonds as a function of the H–H separation. All MBAs from Table 1 are considered.

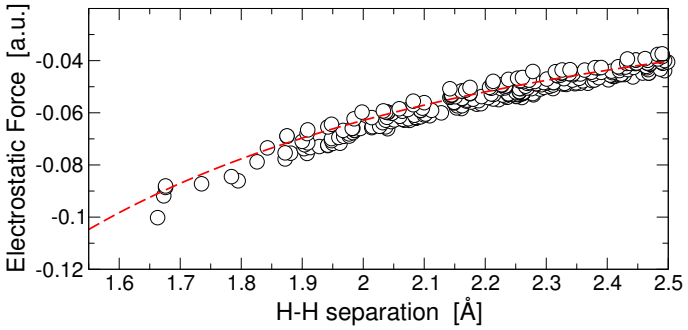

Fig. 5 Modeled electrostatic force between $H^{\delta+}$ and $H^{\delta-}$ of neighboring molecules across all MBAs studied. The dashed red line shows the exact Coulomb interaction calculated from the average $H^{\delta+}$ and $H^{\delta-}$ charges from all MBAs in Table 1. Deviations from the exact interaction are very small.

atom seems to point to an exothermic process. However, reaction energies for the reaction

$$\mathscr{M}(BH_4)_x \cdot yNH_3 \longrightarrow \mathscr{M}(BH_4)_x \cdot (y-z)NH_3 + zNH_3 \qquad (1)$$

are positive, correctly indicating endothermic processes.

The thermodynamic destabilization resulting from ammoniation generally explains the lowering of decomposition temperatures for MBAs observed in Fig. 1. However, it does not explain the increase of decomposition temperatures in high-χ_p MBAs. As a result, we must conclude that high-χ_p MBAs are stabilized kinetically rather than thermodynamically. We discuss the corresponding pathways and kinetics of the decomposition processes in the next section.

3.3 Examining decomposition processes

The processes by which these MBAs decompose have not been clearly determined experimentally. The possible pathways range from simple direct formation of H_2 from $H^{\delta+}$ and $H^{\delta-}$ to very complex interactions forming boron nitrides similar to those found in the decomposition of NH_3BH_3. The observed final products are typically amorphous and poorly characterized. This uncertainty makes the decomposition process difficult to model; without good guidelines from experiment the possible search space is vast.

One recent theoretical study[52] simulated the decomposition of $LiBH_4{\cdot}NH_3$ and $Mg(BH_4)_2{\cdot}2NH_3$ and suggests that the decomposition process begins with the NH_3 drifting away from the $\mathscr{M}(BH_4)_x$, allowing the $\mathscr{M}(BH_4)_x$ to polymerize with its neighbors. Then $H^{\delta+}$ in NH_3 attacks $H^{\delta-}$ from $[BH_4]^-$. While those findings are valuable, it is unclear whether they can be generalized to materials with $\mathscr{M}$ of very different electronegativities. As mentioned in Section 3.1, the direct combination of $H^{\delta+}$ and $H^{\delta-}$ has been suggested to be a possible hydrogen production mechanism in low-χ_p materials,[43] and simulated in a few MBAs,[53] but in high-χ_p materials, the direct H_2 creation pathway would compete with the B_2H_6 creation pathway from the plain MB. B_2H_6 release is always suppressed in the ammoniated materials,[22] but it is not immediately obvious whether this is because the diborane production pathway has been circumvented or because the produced B_2H_6 react immediately with the NH_3. To elucidate these issues, we simulate each of the broad categories mentioned above—NH_3 release, direct H_2 formation, and B_2H_6 formation—and find that each of them becomes the dominating pathway for low-, mid-, and high-χ_p values, respectively.

3.3.1 NH_3 release

Low-χ_p materials release NH_3 preferentially to H_2 or B_2H_6 and some mid-χ_p materials release NH_3 as they are heated before switching to H_2 release—see Fig. 1. In order for an MBA to release NH_3, the NH_3 must escape the metal to which it is coordinated and then escape as a gas.

We quantitatively studied the behavior of the $\mathscr{M}$-NH_3 bond by

Table 2 Pauling electronegativity χ_p, calculated energy of formation ΔE_{atom} [eV per atom], and experimentally observed decomposition temperature T_{dec} [°C] for selected MBAs and their plain MB counterparts, relative to the constituent atoms in their natural states.

MBAs releasing mostly NH_3

Formula	χ_p	ΔE_{atom}	T_{dec}
$Sr(BH_4)_2{\cdot}4NH_3$	0.95	−0.130	14
$Sr(BH_4)_2{\cdot}2NH_3$	0.95	−0.298	130
$Sr(BH_4)_2{\cdot}NH_3$	0.95	−0.432	150
$Sr(BH_4)_2$	0.95	−0.643	400
$Ca(BH_4)_2{\cdot}4NH_3$	1.00	−0.309	85
$Ca(BH_4)_2{\cdot}2NH_3$	1.00	−0.286	160
$Ca(BH_4)_2{\cdot}NH_3$	1.00	−0.414	225
$Ca(BH_4)_2$	1.00	−0.622	380
$Y(BH_4)_3{\cdot}7NH_3$	1.22	−0.069	70
$Y(BH_4)_3{\cdot}6NH_3$	1.22	−0.066	80
$Y(BH_4)_3{\cdot}5NH_3$	1.22	−0.097	110
$Mn(BH_4)_2{\cdot}3NH_3$	1.55	−0.016	80

MBAs releasing mostly H_2

Formula	χ_p	ΔE_{atom}	T_{dec}
$Y(BH_4)_3{\cdot}4NH_3$	1.22	−0.171	165
$Y(BH_4)_3{\cdot}2NH_3$	1.22	−0.316	190
$Y(BH_4)_3{\cdot}NH_3$	1.22	−0.409	195
$Y(BH_4)_3$	1.22	−0.680	200
$Mg(BH_4)_2{\cdot}2NH_3$	1.31	−0.131	205
$Mg(BH_4)_2$	1.31	−0.339	260
$Zr(BH_4)_4{\cdot}8NH_3$	1.33	−0.024	60
$Zr(BH_4)_4$	1.33	−0.423	250
$Mn(BH_4)_2{\cdot}2NH_3$	1.55	−0.074	135
$Mn(BH_4)_2$	1.55	−0.238	155
$Al(BH_4)_3{\cdot}6NH_3$	1.61	−0.057	167
$Al(BH_4)_3$	1.61	−0.345	15
$Zn(BH_4)_2{\cdot}2NH_3$	1.65	−0.087	131
$Zn(BH_4)_2$	1.65	−0.249	−35
$NaZn(BH_4)_3{\cdot}2NH_3$	0.93, 1.65	−0.190	133
$Li_2Mg(BH_4)_4{\cdot}6NH_3$	0.98, 1.31	−0.140	80
$Li_2Al(BH_4)_5{\cdot}6NH_3$	0.98, 1.61	−0.180	138

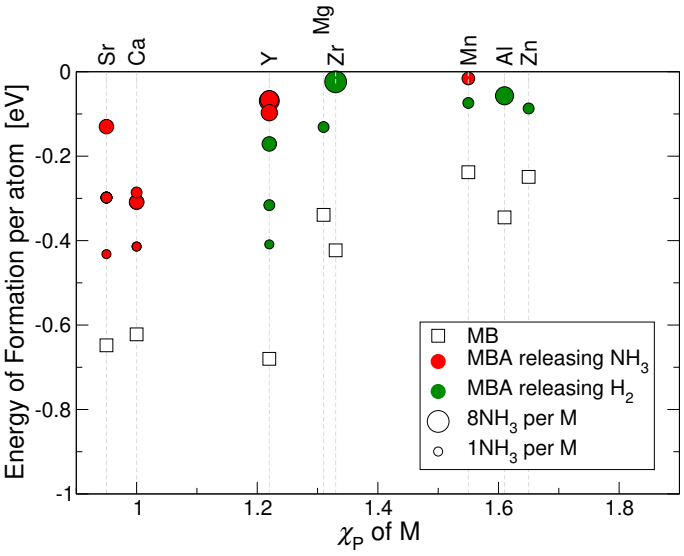

Fig. 6 Energy of formation per atom for pure MBs and MBAs relative to the constituent elements in their natural states. Red and green spots indicate MBAs that release NH_3 and H_2 upon decomposition, respectively. The size of the symbol indicates the number of NH_3 molecules in the material per metal. In all cases studied, the ammoniated MB is destabilized by the addition of the NH_3. See also Table 2.

approximating it as a spring. For small displacements of NH_3 with respect to $\mathscr{M}$, we calculated the total energy of the system and based on the increase in energy relative to the ground state we extracted a spring constant from Hooke's law. The results (depicted in Fig. 7) show that the NH_3 molecules face much steeper potential surfaces in high-χ_p materials, agreeing with the conventional wisdom.[13,45] This means that NH_3 in low-χ_p MBAs can escape more easily, explaining why these materials can decompose at lower temperatures compared to plain MBs by releasing NH_3, whereas the high-χ_p MBAs do not—see Fig. 1. Going from low-χ_p values to higher ones, we also see in Fig. 7 that the NH_3 release becomes energetically more and more expensive, suggesting that eventually there will be a change in decomposition mechanism once an energetically more favorable pathway becomes available.

In addition to NH_3 formation, we must also consider how the NH_3 escapes the material before it can be released as a gas. This kind of process may first occur near the surface of the material, creating vacancy defects in the material. Similarly to how Li^+ diffuses through $LiBH_4$ as it decomposes by hopping between vacancy defects,[29] we suggest that NH_3 may be able to migrate to the surface through such vacancies.

3.3.2 Direct H_2 formation

Direct H_2 formation has been suggested as dehydrogenation pathway[43,53] and can become a more energetically favorable alternative to NH_3 release. We modeled direct H_2 formation from the $H^{\delta+}$ and $H^{\delta-}$ pairs that make up the dihydrogen bond network by generating structures that would be similar to transition states for the reaction. We did this by moving $H^{\delta+}$ and $H^{\delta-}$ from one dihydrogen bond to a separation of 0.74 Å along the axis between them and holding their positions fixed while optimizing the rest of the structure. We did this relaxation for each dihydrogen bond under 2.5 Å; the lowest resulting energies are shown in Fig 8. NEB calculations revealed that there is no kinetic barrier between the ground state structures and the ones that we generated, so we use these energies to approximate the cost of direct H_2 production.

Typically, this procedure resulted in the BH_3 shifting to recapture the $H^{\delta-}$ and the remaining NH_2 shortening its distance to the metal cation, with the net result of a BH_3H_2, and the H_2 would only need to break away from the $[BH_3]^-$ and diffuse out of the material. This result suggests that in an MBA, H is easier to liberate from NH_3 than from $[BH_4]^-$ regardless of the metal's χ_p.

Interestingly, Fig. 8 shows a negative relationship between χ_p and the barrier to direct H_2 creation; while direct H_2 release is very expensive in low-χ_p MBAs, it becomes significantly more favorable for higher-χ_p materials. One important note that may not be evident in the plot is that structures where the metal is directly bound only to NH_3 (e.g. $Zr(BH_4)_4{\cdot}8NH_3$ or $Al(BH_4)_3{\cdot}6NH_3$) tend to have lower-energy transition states than the structures where the $\mathscr{M}(BH_4)_x$ units are maintained. This may have to do with

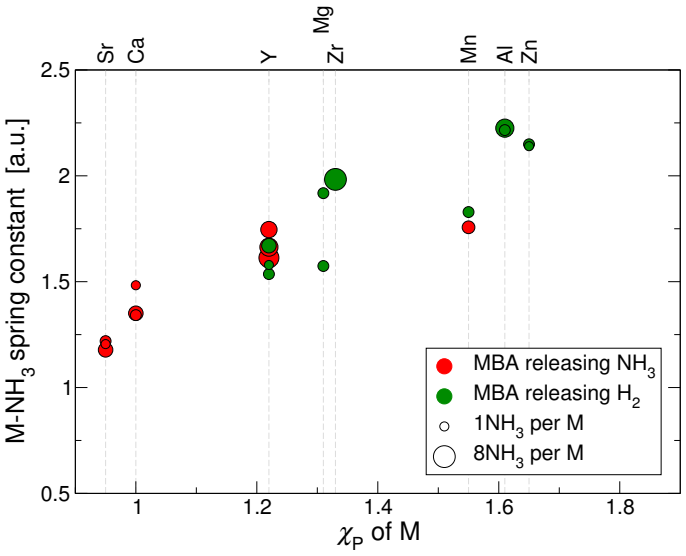

Fig. 7 Average spring constants for the $\mathscr{M}$–NH_3 bond modeled as a harmonic oscillator, as extracted from short fixed-displacement motion. Red and green spots indicate MBAs that release NH_3 and H_2 upon decomposition, respectively. The size of the symbol indicates the number of NH_3 molecules in the material per metal.

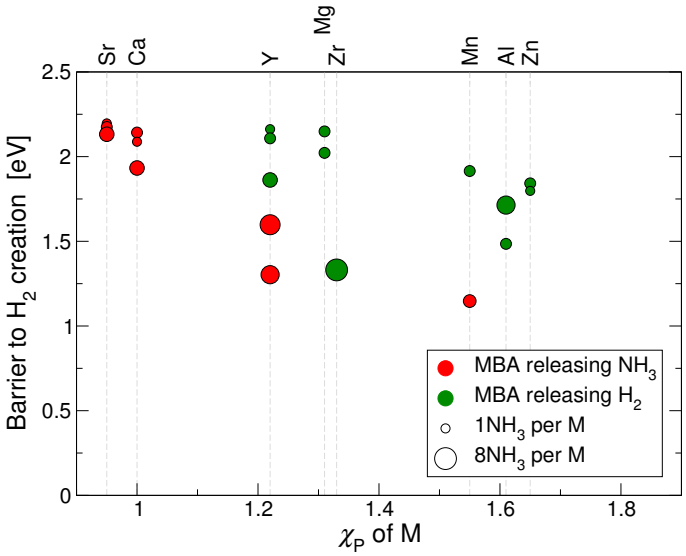

Fig. 8 Estimate of transition state energy for the direct H_2 formation pathway. Red and green spots indicate MBAs that release NH_3 and H_2 upon decomposition, respectively. The symbol size indicates the number of NH_3 molecules in the material per metal.

BH_4 units being less restricted in their movements when they are not coordinated with any particular metal.

In combination with the previous section we conclude that for low-χ_p MBAs the direct H_2 release is energetically expensive (Fig. 8) whereas NH_3 release is favorable (Fig. 7). Going to higher χ_p values, there is a crossover in those two behaviors and for high-χ_p we find that NH_3 release is now energetically very expensive, while direct H_2 release has become more favorable. This crossover nicely explains the shift from NH_3 release to H_2 observed in Fig. 1. However, it does not explain higher decomposition temperatures after ammoniation for high-χ_p materials, which we will further explore in the last section.

3.3.3 B_2H_6 production followed by H_2 release

Up to this point we have found that ammoniation theromodynamically destabilizes *all* MBs. In addition, the previous two sections help understand the shift in release product as a function of χ_p. But, why do high-χ_p MBs with $\mathscr{M}$ = Al and Zn get stabilized upon ammoniation? As we will show, the ammoniation blocks the standard decomposition pathway that these materials prefer, thus kinetically stabilizing those MBAs. We know from the last section that direct H_2 release becomes favorable at mid-χ_p values, but it remains energetically quite expensive. Another pathway for MBAs to decompose is through the formation of B_2H_6. Previous studies show a strong correlation between χ_p,[21] formation enthalpy,[24] and decomposition through B_2H_6 production for MBs. They also show that this pathway opens up for $\chi_p \gtrsim 1.6$, where it becomes—as we will show below—an energetically favorable alternative to direct H_2 formation.

Jepsen and coworkers note that B_2H_6 release is always suppressed in the presence of NH_3, where the two react to form ammine metal borohydrides, suggesting that B_2H_6 may be an intermediate in the H_2 release pathway.[25] These materials have a higher decomposition temperature after the ammoniation process, but at the higher temperature where the MBA begins to decompose, the same B_2H_6 formation process may occur. A very low kinetic barrier of only ~ 0.7 eV was found for the reaction[54]

$$B_2H_6 + NH_3 \longrightarrow NH_2BH_2 + BH_3 + H_2\,, \qquad (2)$$

making B_2H_6 formation followed by H_2 release energetically favorable over direct H_2 formation.

If the kinetic barrier to reaction (2) remains small in the MBA environment, then the only other possible bottleneck in MBA decomposition through the B_2H_6 release pathway is the formation of the B_2H_6 intermediate itself. We performed a transition state search using the NEB method to find the kinetic barriers to B_2H_6 production in selected MBAs, as well as the materials' plain MB counterparts. To find realistic endpoints, we simulated perturbing the system in configuration space by pulling nearby BH_4 units together and allowing the system to relax to a local energy minimum. We performed this process over 250 times and while the relaxations sometimes yielded the desired B_2H_6, it more often resulted in the creation of B_2H_7—a structure that has been observed experimentally[55] and considered as a potential metastable intermediate in $Mg(BH_4)_2$ decomposition.[27] While B_2H_6 can lead to hydrogen release via reaction (2) with a barrier of ~ 0.7 eV, we found no such reaction with B_2H_7. Instead, using NEB calculation we found that the reaction

$$[B_2H_7]^- + NH_3 \longrightarrow NH_3BH_3 + [BH_4]^- \qquad (3)$$

has a barrier of only 0.75 eV relative to the NH_3 and $[B_2H_7]^-$ molecules by themselves in the gas phase—and is thus equally favorable as reaction (2). After this reaction, the NH_3BH_3 is free to decompose on its own (pure NH_3BH_3 decomposes to NH_2BH_2, releasing H_2 at around 100 °C, facing a kinetic barrier of about

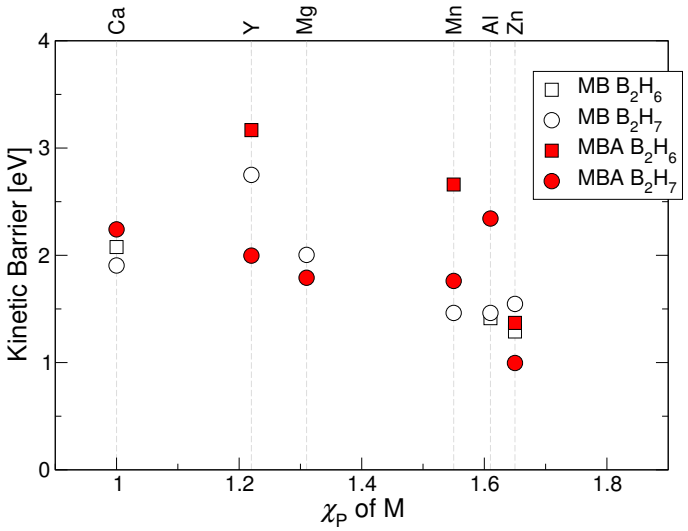

Fig. 9 Kinetic barriers to the formation of B_2H_6 and B_2H_7 in selected pure MBs and MBAs. Barriers for endpoints that were ≥ 3 eV above the ground state structure were not calculated.

1.5 eV in the gas phase[56,57]) or interact further with $[BH_4]^-$ or NH_3. In either case, a similar boron nitride may be formed through the direct H_2 formation pathway.

In addition to the low reaction barrier, any produced borane must diffuse to the surface in order to escape the system. While we have not performed diffusion simulations in these materials, we argue that the kinetic barrier for this diffusion should increase in MBAs because the dihydrogen bond network creates a steeper potential surface that the molecules would need to traverse, potentially trapping the molecules in the material until they react with NH_3.

So, both B_2H_6 and B_2H_7 can eventually produce molecular hydrogen via reactions (2) and (3) with barriers of only ~ 0.7 eV and the formation of B_2H_6 and B_2H_7 themselves might now be the rate-limiting step. We thus calculated and report kinetic barriers to the creation of both B_2H_6 and B_2H_7 in Fig. 9. We did not calculate kinetic barriers to endpoints that we found were ≥ 3 eV above the ground state structure. We find that the kinetic barriers decrease in higher χ_p materials, making this pathway viable for $\chi_p \gtrsim 1.6$, as suggested previously.[21,24] In particular, for these high-χ_p values, this pathway becomes more favorable than direct H_2 release (compare Figs. 8 and 9). It only remains to investigate the effect of ammoniation on this pathway and we analyze the two cases $\mathscr{M}$ = Al and Zn separately.

In $Al(BH_4)_3{\cdot}6NH_3$, the ammoniation drastically increases the barrier for B_2H_7 formation and we could not even find a pathway for B_2H_6 formation. Ammoniation has thus made this decomposition pathway practically inaccessible below the material's decomposition temperature, kinetically stabilizing the Al case. B_2H_6 formation in $Zn(BH_4)_2{\cdot}2NH_3$ faces only a slightly increased barrier upon ammoniation, but a significantly decreased barrier for B_2H_7 formation, pushing the system towards reaction (3). The decomposition is then governed by the hydrogen release from NH_3BH_3, which occurs around 100 °C[56,57] and explains the stabilization seen for Zn in Fig. 1.

The difference between Al and Zn may be due to whether the $[BH_4]^-$ anions are able to transfer H^- as they form B_2H_6. In $Zn(BH_4)_2{\cdot}2NH_3$, the BH_4 are still coordinated with the metal, making the electron transfer simple, but in $Al(BH_4)_3{\cdot}6NH_3$, the NH_3 molecules may act as neutral ligands, preventing reduction of the metal. Roedern and Jensen made a similar assertion in the case of transition-metal MBAs.[16]

The reasons differ for Al and Zn, but in both cases, the B_2H_6 formation pathway that dominates decomposition in the plain MB becomes unavailable after ammoniation, leading to a higher decomposition temperature observed in Fig. 1.

4 Conclusions

We have examined the decomposition processes of MBAs in order to explain why the ammoniation process results in lower decomposition temperatures in materials with low-χ_p metals and higher ones for those with high-χ_p metals.

We found that the dihydrogen bond networks remain very similar between low and high-χ_p materials and cannot explain the sharp distinction between them in terms of the effect of ammoniation. We also found that the ammoniation process always *thermodynamically destabilizes* MBs, while—at the same time—a few high-χ_p materials get *kinetically stabilized* through a shift in decomposition mechanism. We examined three possible decomposition mechanisms: NH_3 release, direct H_2 release, and B_2H_6 or B_2H_7 formation followed by H_2 release. At low-χ_p, NH_3 is weakly bound to the metal and the material decomposes by releasing it. Going to mid-χ_p values, the release of NH_3 becomes less favorable and the materials switch to direct H_2 release, which becomes more favorable with higher χ_p. Finally, for $\chi_p \gtrsim 1.6$, the production of B_2H_6 or B_2H_7 formation becomes more favorable than direct H_2 release, resulting in indirect H_2 release via case-by-case mechanisms. For the special cases of Al and Zn MBs, we further found that this pathway becomes inaccessible upon ammoniation and those phases get kinetically stabilized. In $Al(BH_4)_3{\cdot}6NH_3$, NH_3 shields the metal from being reduced, preventing the electron transfer that occurs in B_2H_6 formation, leaving direct H_2 formation as the only available decomposition pathway. In $Zn(BH_4)_2{\cdot}2NH_3$, B_2H_7 formation becomes more favorable, leading to the formation of NH_3BH_3 rather than B_2H_6. We can thus explain the peculiar stabilization effect of ammoniation in MBs and link it to the exact onset of diborane production.

These insights into how ammoniation affects decomposition processes in MBs can be used to design new mixed-metal MBA materials that decompose in a more desirable fashion or suggest better catalysts for decomposition, perhaps resulting in more reversible hydrogen storage materials.

5 Acknowledgements

This work was supported in full by NSF Grant No. DMR–1145968. T.T. also acknowledges generous support from the Simons Foundation through Grant No. 391888, which endowed his sabbatical at MIT.

References

1 A. Züttel, *Naturwissenschaften*, 2004, **91**, 157–172.

2 J. Graetz, *Chem. Soc. Rev.*, 2009, **38**, 73–82.

3 D. Harrison, E. Welchman, Y. J. Chabal and T. Thonhauser, in *Vol. 5 Energy Storage, Handbook of Clean Energy Systems*, ed. J. Yan, 2015, pp. 2665–2683.

4 M. Dresselhaus, G. Crabtree, M. Buchanan, T. Mallouk, L. Mets, K. Taylor, P. Jena, F. DiSalvo and T. Zawodzinski, *Basic Research Needs for the Hydrogen Economy*, US Department of Energy available at `http://science.energy.gov/~/media/bes/pdf/reports/files/nhe_rpt.pdf`, 2004.

5 *DOE Targets for Onboard Hydrogen Storage Systems for Light-Duty Vehicles*, US Department of Energy available at `http://energy.gov/sites/prod/files/2014/03/f12/targets_onboard_hydro_storage.pdf`, 2009.

6 I. P. Jain, P. Jain and A. Jain, *J. Alloys Compd.*, 2010, **503**, 303–339.

7 H. W. Li, Y. Yan, S. I. Orimo, A. Züttel and C. M. Jensen, *Energies*, 2011, **4**, 185–214.

8 L. H. Rude, T. K. Nielsen, D. B. Ravnsbæk, U. Bösenberg, M. B. Ley, B. Richter, L. M. Arnbjerg, M. Dornheim, Y. Filinchuk, F. Besenbacher and T. R. Jensen, *Phys. Status Solidi Appl. Mater. Sci.*, 2011, **208**, 1754–1773.

9 J. Kostka, W. Lohstroh, M. Fichtner and H. Hahn, *J. Phys. Chem. C*, 2007, **111**, 14026–14029.

10 Y. Yan, A. Remhof, S.-J. Hwang, H.-W. Li, P. Mauron, S.-i. Orimo and A. Züttel, *Phys. Chem. Chem. Phys.*, 2012, **14**, 6514–6519.

11 N. P. Stadie, E. Callini, B. Richter, T. R. Jensen, A. Borgschulte and A. Züttel, *J. Am. Chem. Soc.*, 2014, **136**, 8181–8184.

12 L. Klebanoff and J. Keller, *Int. J. Hydrogen Energy*, 2013, **38**, 4533–4576.

13 L. H. Jepsen, M. B. Ley, Y.-S. Lee, Y. W. Cho, M. Dornheim, J. O. Jensen, Y. Filinchuk, J. E. Jørgensen, F. Besenbacher and T. R. Jensen, *Mater. Today*, 2014, **17**, 129–135.

14 H. Chu, G. Wu, Z. Xiong, J. Guo, T. He and P. Chen, *Chem. Mater.*, 2010, **22**, 6021–6028.

15 Q. Gu, L. Gao, Y. Guo, Y. Tan, Z. Tang, K. S. Wallwork, F. Zhang and X. Yu, *Energy Environ. Sci.*, 2012, **5**, 7590–7600.

16 E. Roedern and T. R. Jensen, *Inorg. Chem.*, 2015, **54**, 10477–10482.

17 W. Sun, X. Chen, Q. Gu, K. S. Wallwork, Y. Tan, Z. Tang and X. Yu, *Chem. Eur. J.*, 2012, **18**, 6825–6834.

18 F. Yuan, Q. Gu, Y. Guo, W. Sun, X. Chen and X. Yu, *J. Mater. Chem.*, 2012, **22**, 1061–1068.

19 J. Huang, L. Ouyang, Q. Gu, X. Yu and M. Zhu, *Chem. Eur. J.*, 2015, **21**, 14931–14936.

20 J. Huang, Y. Tan, Q. Gu, L. Ouyang, X. Yu and M. Zhu, *J. Mater. Chem. A*, 2015, **3**, 5299–5304.

21 Y. Nakamori, K. Miwa, A. Ninomiya, H. Li, N. Ohba, S.-i. Towata, A. Züttel and S.-i. Orimo, *Phys. Rev. B*, 2006, **74**, 045126.

22 L. H. Jepsen, M. B. Ley, R. Černý, Y.-S. Lee, Y. W. Cho, D. Ravnsbæk, F. Besenbacher, J. Skibsted and T. R. Jensen, *Inorg. Chem.*, 2015, **54**, 7402–7414.

23 G. Soloveichik, J.-H. Her, P. W. Stephens, Y. Gao, J. Rijssenbeek, M. Andrus and J.-C. Zhao, *Inorg. Chem.*, 2008, **47**, 4290–4298.

24 D. Harrison and T. Thonhauser, *Int. J. Hydrogen Energy*, 2016, **41**, 3571–3578.

25 L. H. Jepsen, Y.-S. Lee, R. Černý, R. S. Sarusie, Y. W. Cho, F. Besenbacher and T. R. Jensen, *ChemSusChem*, 2015, **8**, 3472–3482.

26 S. Li, M. Willis and P. Jena, *J. Phys. Chem. C*, 2010, **114**, 16849–16854.

27 Y. Zhang, E. Majzoub, V. Ozoliņš and C. Wolverton, *J. Phys. Chem. C*, 2012, **116**, 10522–10528.

28 K. Hoang, A. Janotti and C. G. Van De Walle, *Phys. Rev. B - Condens. Matter Mater. Phys.*, 2012, **85**, 1–12.

29 K. Hoang and C. G. V. de Walle, *Int. J. Hydrogen Energy*, 2012, **37**, 5825–5832.

30 G. Kresse and J. Furthmüller, *Phys. Rev. B*, 1996, **54**, 11169–11186.

31 G. Kresse and D. Joubert, *Phys. Rev. B*, 1999, **59**, 1758–1775.

32 J. Klimeš, D. R. Bowler and A. Michaelides, *Phys. Rev. B*, 2011, **83**, 195131.

33 T. Thonhauser, V. R. Cooper, S. Li, A. Puzder, P. Hyldgaard and D. C. Langreth, *Phys. Rev. B*, 2007, **76**, 125112.

34 D. C. Langreth, B. I. Lundqvist, S. D. Chakarova-Käck, V. R. Cooper, M. Dion, P. Hyldgaard, A. Kelkkanen, J. Kleis, L. Kong, S. Li, P. G. Moses, E. D. Murray, A. Puzder, H. Rydberg, E. Schröder and T. Thonhauser, *J. Phys. Condens. Matter*, 2009, **21**, 084203.

35 K. Berland, V. R. Cooper, K. Lee, E. Schröder, T. Thonhauser, P. Hyldgaard and B. I. Lundqvist, *Reports Prog. Phys.*, 2015, **78**, 066501.

36 T. Thonhauser, S. Zuluaga, C. A. Arter, K. Berland, E. Schröder and P. Hyldgaard, *Phys. Rev. Lett.*, 2015, **115**, 136402.

37 G. Henkelman, B. P. Uberuaga and H. Jónsson, *J. Chem. Phys.*, 2000, **113**, 9901–9904.

38 G. Henkelman and H. Jónsson, *J. Chem. Phys.*, 2000, **113**, 9978–9985.

39 D. Harrison and T. Thonhauser, *Phys. Rev. B*, 2014, **90**, 125152.

40 J. Huang, Y. Tan, J. Su, Q. Gu, R. Černý, L. Ouyang, D. Sun, X. Yu and M. Zhu, *Chem. Commun.*, 2015, **51**, 2794–2797.

41 D. B. Ravnsbæk, E. A. Nickels, R. Černý, C. H. Olesen, W. I. F. David, P. P. Edwards, Y. Filinchuk and T. R. Jensen, *Inorg. Chem.*, 2013, **52**, 10877–10885.

42 L. H. Rude, M. Corno, P. Ugliengo, M. Baricco, Y.-S. Lee, Y. W. Cho, F. Besenbacher, J. Overgaard and T. R. Jensen, *J. Phys. Chem. C*, 2012, **116**, 20239–20245.

43 L. H. Jepsen, M. B. Ley, Y. Filinchuk, F. Besenbacher and T. R. Jensen, *ChemSusChem*, 2015, **8**, 1452–1463.

44 E. H. Majzoub and E. Rönnebro, *J. Phys. Chem. C*, 2009, **113**, 3352–3358.

45 Z. Tang, Y. Tan, H. Wu, Q. Gu, W. Zhou, C. M. Jensen and X. Yu, *Acta Mater.*, 2013, **61**, 4787–4796.

46 G. Xia, Q. Gu, Y. Guo and X. Yu, *J. Mater. Chem.*, 2012, **22**, 7300–7307.

47 Y. Yang, Y. Liu, H. Wu, W. Zhou, M. Gao and H. Pan, *Phys. Chem. Chem. Phys.*, 2014, **16**, 135–143.

48 Y. Guo, H. Wu, W. Zhou and X. Yu, *J. Am. Chem. Soc.*, 2011, **133**, 4690–4693.

49 T. Sato, K. Miwa, Y. Nakamori, K. Ohoyama, H.-W. Li, T. Noritake, M. Aoki, S.-i. Towata and S.-i. Orimo, *Phys. Rev. B*, 2008, **77**, 104114.

50 R. F. W. Bader, *Atoms in Molecules: A Quantum Theory*, 1990.

51 G. Henkelman, A. Arnaldsson and H. Jónsson, *Comp. Mater. Science*, 2006, **36**, 354–360.

52 K. Wang, J.-G. Zhang and X.-Q. Lang, *Phys. Chem. Chem. Phys.*, 2016, **18**, 7015–7018.

53 X. Chen and X. Yu, *J. Phys. Chem. C*, 2012, **116**, 11900–11906.

54 V. S. Nguyen, M. H. Matus, M. T. Nguyen and D. A. Dixon, *J. Phys. Chem. A*, 2008, **112**, 9946–9954.

55 S. G. Shore, S. H. Lawrence, M. I. Watkins and R. Bau, *J. Am. Chem. Soc.*, 1982, **104**, 7669–7670.

56 S. A. Shevlin, B. Kerkeni and Z. X. Guo, *Phys. Chem. Chem. Phys.*, 2011, **13**, 7649–7659.

57 E. Welchman and T. Thonhauser, *J. Mater. Chem. A*, 2015, **3**, 18528–18534.